Appl. Phys. B 75, 595–599 (2002)
DOI: 10.1007/s00340-002-1036-z

Applied Physics B
Lasers and Optics

W. LIU[1,✉]
O. KOSAREVA[2]
I.S. GOLUBTSOV[2]
A. IWASAKI[1]
A. BECKER[3,4]
V.P. KANDIDOV[2]
S.L. CHIN[1]

Random deflection of the white light beam during self-focusing and filamentation of a femtosecond laser pulse in water

[1] Departement de Physique, de Génie Physique et d'Optique et Centre d'Optique, Photonique et Laser, Université Laval, Québec, G1K 7P4 Canada
[2] International Laser Center, Physics Department, Moscow State University, Moscow, 119992, Russia
[3] Fakultät für Physik, Universität Bielefeld, Postfach 100 131, 33501 Bielefeld, Germany
[4] Max-Planck-Institut für Physik Komplexer Systeme, Nöthnitzer Strasse 38, 01187 Dresden, Germany

Received: 13 June 2002/Revised version: 16 August 2002
Published online: 25 October 2002 •

ABSTRACT Ti:sapphire femtosecond laser pulse filamentation in competition with optical breakdown in condensed matter is studied both experimentally and numerically using water as an example. Strong random deflection and modulation of the supercontinuum under tight focusing conditions were observed. They manifest the beginning of the filamentation process near the highly disordered plasma created by optical breakdown at the geometrical focus.

PACS 52.38.Hb; 42.65.Jx; 42.65.Tg; 33.80.Wz; 52.35.Mw

1 Introduction

Recently, it became possible to write waveguides inside optical materials using infrared femtosecond laser pulses [1–4]. For the successful technological development of writing such kinds of waveguides towards a use in integrated optics, it is important to understand the interaction between a femtosecond laser and different optical materials. Laser induced optical breakdown and laser pulse filamentation are the main non-linear processes during waveguide writing.

Filamentation usually occurs during the propagation of a powerful ultrashort laser pulse in all kinds of optical materials such as gases, liquids and solids (e.g. [5–13]). It is the result of a balance between a number of non-linear processes, mainly the Kerr self-focusing of the laser pulse and the defocusing effect of the plasma generated at high intensities in the self-focal region due to multiphoton/tunnel ionization in gases or multiphoton excitation of electrons to the conduction band in condensed matter. The filamentation process is accompanied by a strong broadening of the laser spectrum, which can extend from the near-infrared to the visible, due to self-phase modulation and self-steepening [14, 15]. This is called a super-continuum (SC) [16] or white-light laser [17].

The plasma density needed to balance the self-focusing was found to be much lower than the material density [18]. However, such a weak plasma already changes the refractive index of the optical material, resulting in the filamentation process, but avoids damage inside the condensed matter. In contrast, optical breakdown appears to be due to multiphoton and avalanche ionization induced by the laser under tight focusing conditions and the breakdown plasma is usually so strong that real damage to the material occurs. Thus, the filamentation process seems to potentially open a more promising way to write high-quality waveguides than optical breakdown.

✉ Fax: +1-418/656-2623, E-mail: wliu@phy.ulaval.ca

Laser-induced breakdown produced by femtosecond pulses in water has been discussed in several papers (e.g. [19–23]). In particular, these works address experimental and theoretical studies of the breakdown threshold dependence on the pulse duration, energy, wavelength, geometry of the experiment and additives in the sample. According to [19, 20], the optical breakdown in water can be identified as the appearance of the residual bubbles that takes place when the free electron density reaches approximately $10^{18}\,\mathrm{cm}^{-3}$. Time-resolved shadow imaging of the breakdown-induced refractive index modifications in water indicates the presence of filamentation [23]. The authors of [23] briefly mention the presence of randomly distributed white light spots over the transverse beam profile, which is evidence of the spectral broadening of a 100-fs laser pulse in water. At the same time, the investigation of the joint manifestation of such non-linear processes as self-focusing and multiphoton ionization continued by avalanche ionization in the course of geometrical focusing of a femtosecond pulse into the water cell has not been presented in the literature so far.

We have studied both experimentally and numerically the competition of laser-pulse filamentation and laser-induced optical breakdown in water as an example of condensed matter under different focusing conditions. The detailed results will be given elsewhere. In advance, we report in this short communication the observation of a strong

deflection and modulation of the white-light beam, which characterizes the appearance of the filament near the strong, highly disordered optical breakdown plasma.

2 Experimental set-up and results

The experimental set-up is schematically illustrated in Fig. 1. The laser pulses were generated by a chirped-pulse-amplification (CPA) Ti:sapphire laser system, which included a Ti:sapphire oscillator (Spectra Physics Maitai, 300 mW, 80 MHz) followed by a CPA regenerative amplifier (Spectra Physics Spitfire) at 1 kHz repetition rate and a compressor. The laser pulses centered at $\lambda_0 = 810$ nm with 45-fs pulse duration (FWMH, measured by a Positive Light single shot auto-correlater) and a beam diameter of 5 mm ($1/e^2$). The beam was focused by a microscope objective into a glass water cell of 2 cm in length as well as in diameter, while the windows of the cell were 1 mm thick. The geometrical focus was located at the center of the cell. In the forward direction, the generated white-light beam was collected by two lenses (both with $f = 6$ cm) onto a photodiode (PD). The signal of the photodiode was observed on an oscilloscope. A Bg12 blue filter and a 0° incident angle dielectric mirror (with ∼ 100% reflectivity around 800 nm) were used in order to filter the strong laser spectrum and the optical breakdown spectrum around 810 nm.

We used two microscope objectives with focal lengths of $f = 16.9$ mm and $f = 30.8$ mm. The laser input energy was chosen to be 3.0 μJ, which was found to be equal to the threshold for laser-pulse filamentation and supercontinuum generation for the $f = 16.9$ mm microscope objective, but to exceed the respective threshold for the longer focal length (2.3 μJ). We further observed at this input energy for both microscope objectives the appearance of a strong optical breakdown at the geometrical focus. Note that the glass window of the water cell did not influence the beam propagation significantly. It has been shown [24] for similar input parameters that laser-beam filamentation and strong ionization within a 1 mm glass plate occurs only when the beam radius does not exceed 30 μm. In the present experiment, the minimum beam radius at the entrance of the window was 812 μm and, hence, far above this limit. The influence of the glass window on the results presented below is therefore negligible.

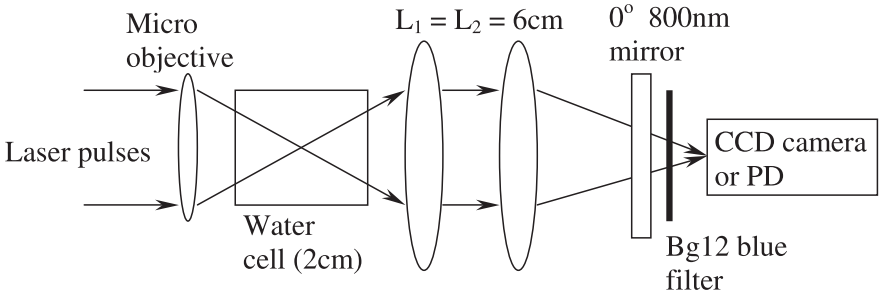

FIGURE 1 The experimental set-up

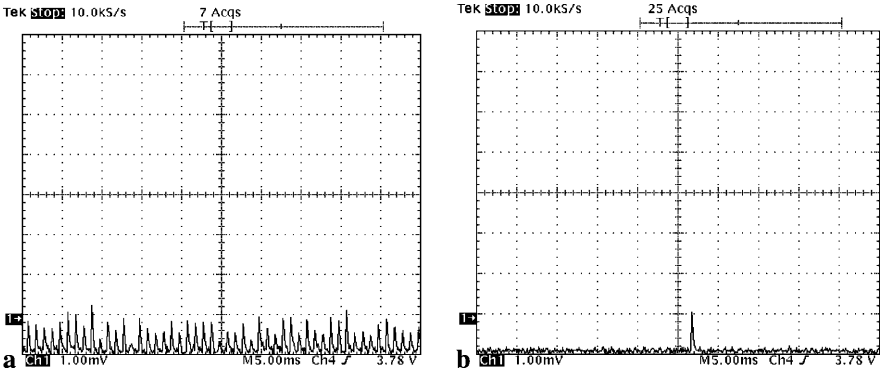

FIGURE 2 Oscilloscope signal at an input energy of 3 μJ for microscope objectives with focal lengths $f = 30.8$ mm (**a**) and $f = 16.9$ mm (**b**)

The signals detected on the oscilloscope for (a) the $f = 30.8$ mm microscope objective and (b) the $f = 16.9$ mm microscope objective are shown in Fig. 2. The signals strongly differ in their appearance frequencies. While for the longer focal length the frequency equals 1 kHz, corresponding to the laser repetition rate, it drops to less than 20 Hz for the microscope objective with the shorter focal length. In the latter case, we further observed by eye during the experiment a random appearance of the SC white-light beam at cone angles of up to ±40° with respect to the laser propagation direction. We characterize this observation as a jumping or moving white-light behavior. When the SC occurs randomly at different angles, it will hit the small opening of the photodiode very rarely, as detected on the oscilloscope (Fig. 2b). We also used a large-detector-area (8.8 mm × 6.6 mm) CCD camera to record all the moving white-light shots. The camera worked at 25 frames per second and could be video triggered. During a period of 5 min, 54 shots were recorded, and 253 shots were recorded in 30 min. The jumping behavior of the white-light beam was further accompanied by a random distribution of the color components inside the SC.

3 Numerical simulations

In order to provide an explanation of the moving white-light behaviour, we performed numerical simulations for the non-linear laser beam propagation in water. Our theoretical model was based on the wave equation for the slowly-varying-envelope approximation coupled to the equation for the free-electron density. A similar system of equations was used earlier for the description of the filamentation in air [25]. Assuming propagation along the z-axis with group velocity v_g, the electric field envelope $E(r, z, t)$ is determined via the equation

$$2ik\left(\frac{\partial E}{\partial z}+\frac{1}{v_g}\frac{\partial E}{\partial t}\right)=\Delta_\perp E - kk''_\omega\frac{\partial^2 E}{\partial t^2}+\frac{2k^2}{n_0}(\Delta n_k+\Delta n_p)E - ik\alpha E\,, \quad (1)$$

where the first and the second terms on the right-hand side describe diffraction

and group velocity dispersion. The nonlinearity is given by the instantaneous Kerr contribution

$$\Delta n_k = \frac{1}{2} n_2 |E|^2 \tag{2}$$

and the plasma contribution

$$\Delta n_\mathrm{p} = \frac{1}{2}\left(\frac{\omega_\mathrm{p}^2}{\omega^2 + v_\mathrm{c}^2} + i\frac{v_\mathrm{c}}{\omega}\frac{\omega_\mathrm{p}^2}{\omega^2 + v_\mathrm{c}^2}\right). \tag{3}$$

Here, E is the electric field amplitude, ω is the laser central frequency, $\omega_\mathrm{p}^2 = \frac{4\pi e^2 N_\mathrm{e}}{m}$ is the plasma frequency and $N_\mathrm{e}(r, z, t)$ is the free-electron density, determined by

$$\frac{\partial N_\mathrm{e}}{\partial t} = R(|E|^2)(N_\mathrm{a} - N_\mathrm{e}) + v_\mathrm{i} N_\mathrm{e} - \beta N_\mathrm{e}^2, \tag{4}$$

with the density of neutrals $N_\mathrm{a} = 3.3 \times 10^{22}\,\mathrm{cm}^{-3}$ and the avalanche ionization frequency $v_\mathrm{i} = \frac{1}{W_\mathrm{g}} \frac{e^2 E^2}{2m(\omega^2 + v_\mathrm{c}^2)} v_\mathrm{c}$. $W_\mathrm{g} = 6.5\,\mathrm{eV}$ is the band gap energy and $v_\mathrm{c} = N_\mathrm{a} v_\mathrm{e} \sigma_\mathrm{c}$ is the electron collision frequency with the root-mean-square electron velocity v_e and the electron collision cross section $\sigma_\mathrm{c} = 10^{-15}\,\mathrm{cm}^2$ [26]. m and e are the electron mass and charge, respectively. The optical-field-induced ionization rate $R(|E|^2)$ depending on the light intensity is calculated according to [27]. The radiative electron recombination coefficient is given by [26]:

$$\beta = \frac{8.75 \times 10^{-27}}{T^{9/2}} N_\mathrm{e}\ [\mathrm{cm}^3/\mathrm{s}], \tag{5}$$

where T is the electron temperature in the laser-produced plasma in eV. The last term on the right-hand side of (1) describes the energy losses due to electron transitions to the conduction band. α is the energy-loss coefficient due to multiphoton ionization. The group velocity dispersion coefficient was $k''_\omega \approx 5 \times 10^{-28}\,\mathrm{s}^2/\mathrm{cm}$ [28]. The non-linear refractive index coefficient was calculated from the critical power for self-focusing obtained from the experiment as $n_2 = 2 \times 10^{-16}\,\mathrm{cm}^2/\mathrm{W}$ [10].

In the simulations, the parameters and the geometry of the propagation were chosen to correspond to those used in the measurements. The pulse at the entrance to the water cell was chosen to be Gaussian in space and time with a pulse length of 45 fs (FWHM). Linear propagation in air was assumed and the focal distance in water was chosen as 1 cm.

The results of the simulations for an initial pulse energy of 3.0 μJ and focal distances of (a) $f = 30.8\,\mathrm{mm}$ and (b) $f = 16.9\,\mathrm{mm}$, as in the experiment, are presented in Fig. 3. The upper plot in each panel shows the change of the fluence distribution with distance, while the lower plot shows the change of the electron density as a function of the position along the water cell with respect to the geometrical focal point at 0 mm.

At the beginning of the water cell, the propagation of the pulse is mainly defined by the geometrical focusing. As the pulse approaches the geometrical focus, self-focusing starts to contribute to the pulse transformation. The fluence distribution in the plane $\{r, z\}$ has a sickle-shaped structure with the first maximum located in the non-linear focal position z'_f calculated for the focused beam undergoing self-focusing [29]. This indicates the start of the area with the large value of fluence and we will refer to this area with $z > z'_f$ as to the filament.

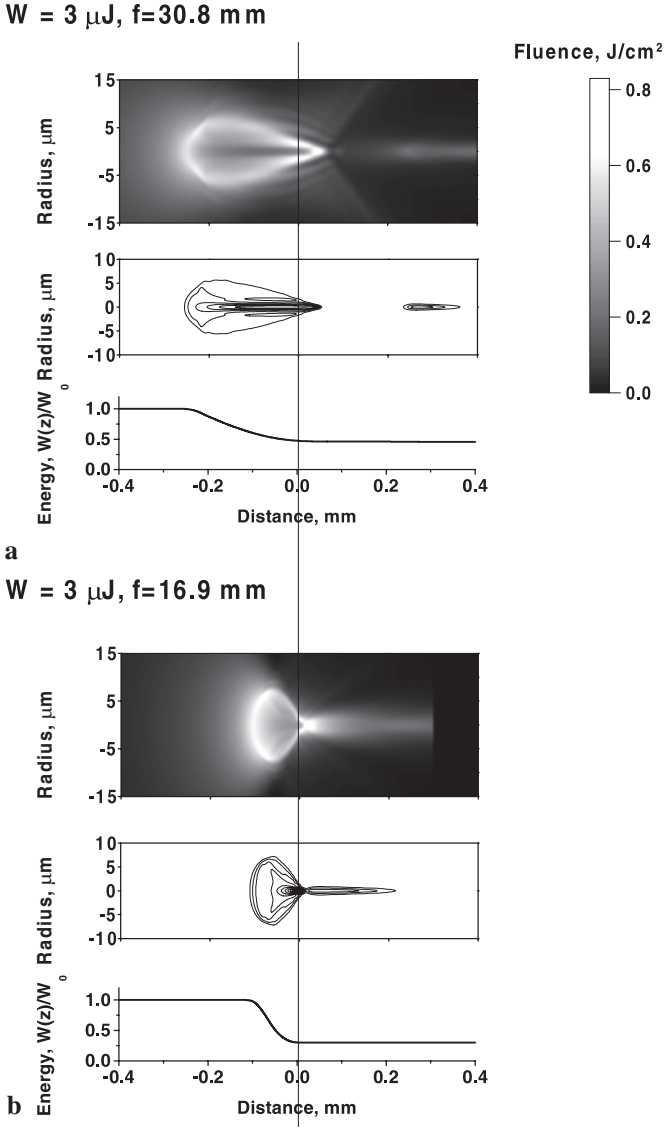

FIGURE 3 The simulated evolution of the fluence distribution (*upper plots*) and the electron density distribution (*lower plots*) as a function of the propagation axis z in the water cell. The geometric focus position ($z = 0.0$ mm) is indicated by the *vertical solid line*. The initial pulse energy is $W = 3$ μJ. The interval between the electron density contours in **a** and **b** is $\Delta N_\mathrm{e} = 0.002 N_\mathrm{a}$. **a** The focal length of the lens is $f = 30.8$ mm, the maximum electron density is $N_{\mathrm{e\ max}} = 0.012 N_\mathrm{a}$; and **b** $f = 16.9$ mm, $N_{\mathrm{e\ max}} = 0.025 N_\mathrm{a}$

In the case of a lens with the focal lens $f = 30.8$ mm (Fig. 3a), self-focusing essentially contributes to the spatial–temporal contraction of the pulse. The non-linear focus position $z = z'_f$ and the geometrical focus $z = 0$ are well separated, a stable plasma channel for the filament starts to be formed.

For the shorter focal length lens $f =$ 16.9 mm (Fig. 3b), the major contribution to the pulse contraction is due to the geometrical focusing, and the plasma formation is governed by the geometrical convergence of the whole beam. The separation between the non-linear focus position $z = z'_f$ and the geometrical focus position $z = 0$ is smaller in comparison with the focal lens $f = 30.8$ mm.

The transverse size of the fluence and the plasma increases with decreasing geometrical focal length. For $f =$ 30.8 mm, this transverse size defined at the level $10^{-3}N_a$ is 11 μm ($z = -0.18$ mm, Fig. 3a) while for $f =$ 16.9 mm it is 14 μm ($z = -0.06$ mm, Fig. 3b). The essential difference is in the maximum electron density value, which is $0.025N_a$ for $f = 16.9$ mm and two-times lower for $f = 30.8$ mm. For both geometrical focal lengths, the electron density maximum is attained right before the geometrical focus at $z \approx -0.04$ mm in Fig. 3a and at $z \approx -0.003$ mm in Fig. 3b.

Let us now compare our simulation results with the results obtained from a model based on a similar system of equations for pulse propagation and plasma generation [21], except that the optical-field induced ionization in [21] is described by a power law, while we used an ionization rate [27]. The input pulse parameters in [21] differ from ours; the input pulse duration was 200 fs, the wavelength 580 nm, the ratio $f/d \approx 70$ and the ratio $P/P_{crit} \approx 1$ (P is the input pulse peak power and P_{crit} is the critical power for self-focusing in water) instead of 45 fs, 810 nm, $f/d \approx$ 3.4–14 and $P/P_{cr} \approx 15$ used in this paper. Although quantitative comparison is hard to do, the peak intensity reached in [21] is 6×10^{12} W/cm^2, which is in reasonable agreement with our peak intensity of 2×10^{13} W/cm^2 at $P/P_{crit} \approx 1$, bearing in mind the shorter pulse duration and the higher multiphoton ionization threshold due to the longer laser wavelength in the present paper. Also, our simulations show qualitatively the same main features for the spatio–temporal dynamics of the pulse, which is typical for a medium with self-focusing, ionization and group velocity dispersion, namely the formation of a sharp peak in the front, divergence of the pulse part following the leading peak, and pulse splitting. At the same time, we found that this dynamics crucially depended on the geometrical focusing conditions and pulse energy. A detailed study of this dependence will be presented in the longer publication.

The change of the fluence and the corresponding plasma distribution with the change in the focal length of the lens demonstrates the joint manifestation of the filamentation and optical breakdown for different geometries of the experiment. Tight focusing leads to large transverse and small longitudinal sizes of the fluence and plasma in combination with high values of the maximum electron density. To the contrary, weaker focusing leads to smaller transverse, but larger longitudinal sizes of the fluence and the plasma, i.e. the filamentation is more pronounced. At the same time, the values of the maximum plasma density are lower.

In Fig. 4 we present the transverse distributions of the laser intensity in the leading (dashed curves) and trailing parts (solid curves) of the pulse for

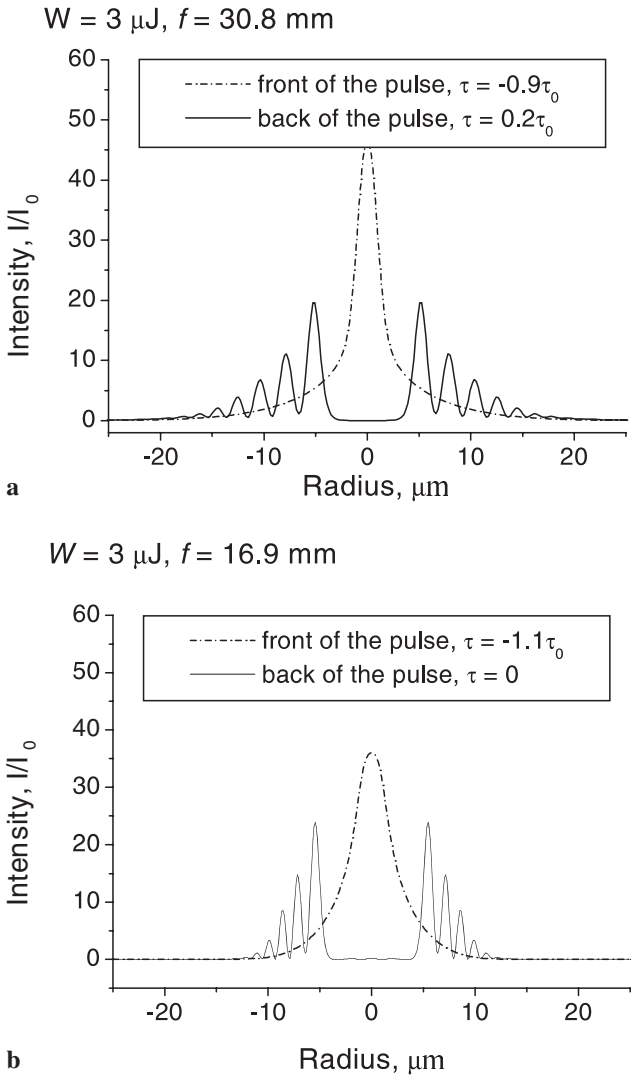

FIGURE 4 The simulated transverse intensity distributions in the vicinity of the geometrical focus. For both panels, the dash–dotted line is the intensity at the front of the pulse, and the solid line is the intensity at the back of the pulse. The slice in the front of the pulse is chosen so that the pulse intensity takes its maximum at this retarded time moment. The slice at the back of the pulse is separated from the front slice by the time interval $1.1\tau_0$ for both panels (**a**) and (**b**). The geometrical focal position is at $z = 0.0$ mm, $I_0 = 10^{12}$ W/cm^2. **a** $f = 30.8$ mm, $z = -0.12$ mm; and **b** $f = 16.5$ mm, $z = -0.05$ mm

(a) $f = 30.8$ mm and (b) $f = 16.9$ mm. In the front of the pulse, the intensity maximum is on-axis, while at the back of the pulse a ring structure is created, which essentially contributes to the generation of the supercontinuum [30–32]. For the shorter focal length (panel b) a strong convergence of the beam takes place and the ring structure is more intense than for the $f = 30.8$ mm focal length.

We are now in a position to explain the moving white-light spot, which we observed for the short-focal-length lens ($f = 16.9$ mm). The white light is generated due to self-phase modulation in the plasma [25] at the back of the pulse following the high-intensity front, which creates the plasma at the geometrical focus. Therefore, it is this plasma at the geometrical focus that can deflect the white light from its forward propagation.

Our simulations show that at the geometrical focus, the high electron density ($> 10^{20}\,\mathrm{cm}^{-3}$) produced by a 3 μJ pulse focused with a 16.9 mm lens is mainly due to the contribution from avalanche ionization (i.e. the second term in (4)), while electrons generated by multiphoton ionization constitute approximately one sixth of the total electron density only. We may therefore refer to the plasma near the geometrical focus as the optical breakdown (OB) plasma.

The simulations further show that the shorter the focal length, the larger is the transverse size of the OB plasma. In the experiment, due to fluctuations in the input pulse intensity and energy from shot to shot, this transverse area is unstable with respect to the initial localization of the plasma formation. Thus, the large transverse size and the instability of the OB plasma lead to a random deviation of the white-light beam in the case of the short focal length ($f = 16.9$ mm), which is manifested by a decrease in the repetition rates of the white-light signal (Fig. 2b), the appearance of the jumping behavior of the white light and the random color distribution inside the SC, as observed in the experiment. Note that numerical simulations of the jumping white-light phenomenon is a challenging task, because cylindrical geometry and paraxial approximation do not work in this situation. Therefore, we have to limit ourselves here to this qualitative explanation.

In the case of the longer geometrical focal length, our simulations show that the transverse size of the OB plasma is smaller. The self-focusing, which has a larger effect on propagation in the case of longer geometrical focus, drives in this case the initial localization of the plasma towards the beam axis. The white light is generated along the comparatively long filament and deflected at a small constant angle only. Experimentally, we consistently observed the forward propagation of the white-light pulse (Fig. 2a).

4 Conclusion

We have investigated both experimentally and numerically the creation of a filament in a femtosecond laser pulse focused in water, as an example of condensed matter. We observed the appearance of a randomly distributed white-light beam as a characteristic signature for the appearance of filamentation and supercontinuum generation near the breakdown plasma at the geometrical focus.

ACKNOWLEDGEMENTS This work was partially supported by NATO, NSERC, DRDC-Valcartier, le Fonds FCAR, CIPI, Canada Research Chairs, the Alexander von Humboldt Foundation, DFG and the Russian Fund for Basic Research. The collaboration of Spectra Physics/Positive Light in setting up the versatile laser system in Laval University is particularly appreciated.

REFERENCES

1 K.M. Davis, K. Miura, N. Sugimoto, K. Hirao: Opt. Lett. **21**, 1729 (1996)
2 K. Hirao, K. Miura: J. Non-Cryst. Sol. **239**, 91 (1998)
3 L. Sudrie, M. Franco, B. Prade, A. Mysyrowicz: Opt. Commun. **191**, 333 (2001)
4 K. Yamada, W. Watanabe, T. Toma, K. Itoh, J. Nishii: Opt. Lett. **26**, 19 (2001)
5 E. Yablonovitch, N. Bloembergen: Phys. Rev. Lett. **29**, 907 (1972)
6 W. Lee Smith, P. Liu, N. Bloembergen: Phys. Rev. A **15**, 2396 (1977)
7 P.B. Corkum, C. Rolland, T. Srinivasan-Rao: Phys. Rev. Lett. **57**, 2268 (1986)
8 A. Braun, G. Korn, X. Liu, D. Du, J. Squier, G. Mourou: Opt. Lett. **20**, 73 (1995)
9 L. Wöste, C. Wedekind, H. Wille, P. Rairoux, B. Stein, S. Nikolov, C. Werner, S. Niedermeier, F. Ronneberger, H. Schillinger, R. Sauerbrey: Laser Optoelektronik **29**, 51 (1997)
10 A. Brodeur, S.L. Chin: Phys. Rev. Lett. **80**, 4406 (1998)
11 A. Brodeur, S.L. Chin: J. Opt. Soc. Am. B **16**, 637 (1999)
12 R. Rairoux, H. Schillinger, S. Niedermeier, M. Rodriguez, F. Ronneberger, R. Sauerbrey, B. Stein, D. Waite, C. Wedekind, H. Wille, L. Wöste, C. Ziener: Appl. Phys. B **71**, 573 (2000)
13 W. Liu, S. Petit, A. Becker, N. Aközbek, C.M. Bowden, S.L. Chin: Opt. Commun. **202**, 189 (2002)
14 N. Aközbek, M. Scalora, C.M. Bowden, S.L. Chin: Opt. Commun. **191**, 353 (2001)
15 A.L. Gaeta: Phys. Rev. Lett. **84**, 3582 (2000)
16 R.R. Alfano (Ed.): *The Supercontinuum Laser Source* (Springer, New York 1989)
17 S.L. Chin, A. Brodeur, S. Petit, O.G. Kosareva, V.P. Kandidov: J. Nonlinear Opt. Phys. Mat. **8**, 121 (1999)
18 J. Kasparian, R. Sauerbrey, S.L. Chin: Appl. Phys. B **71**, 877 (2000)
19 P.K. Kennedy, S.A. Boppart, D.X. Hammer, B.A. Rockwell, G.D. Noojin, W.P. Roach: IEEE J. Quantum Electron. **QE31**, 2250 (1995)
20 D.X. Hammer, R.J. Thomas, G.D. Noojin, B.A. Rockwell, P.K. Kennedy, W.P. Roach: IEEE J. Quantum Electron. **QE32**, 670 (1996)
21 Q. Feng, J.V. Moloney, A.C. Newell, E.M. Wright, K. Cook, P.K. Kennedy, D.X. Hammer, B.A. Rockwell, C.R. Thompson: IEEE J. Quantum Electron. **QE33**, 127 (1997)
22 A. Vogel, J. Noack, K. Nahen, D. Theisen, S. Busch, U. Parlitz, D.X. Hammer, G.D. Noojin, B.A. Rockwell, R. Birngruber: Appl. Phys. B **68**, 271 (1999)
23 E. Abraham, K. Minoshima, H. Matsumoto: Opt. Commun. **176**, 441 (2000)
24 S. Tzortzakis, L. Sudrie, M. Franco, B. Prade, A. Mysyrowiez: Phys. Rev. Lett. **87**, 213 902 (2001)
25 O.G. Kosareva, V.P. Kandidov, A. Brodeur, S.L. Chin: J. Nonlinear Opt. Phys. Mat. **6**, 485 (1997)
26 Y.P. Raizer: *Gas Discharge Physics* (Springer-Verlag, New York 1991)
27 A.M. Perelemov, V.S. Popov, M.V. Terent'ev: Sov. Phys. JETP **23**, 924 (1966)
28 *Handbook of Chemistry and Physics* (CRC Press, 1984–1985)
29 J.H. Marburger: Prog. Quantum Electron. **4**, 35 (1975)
30 S.C. Rae: Opt. Commun. **104**, 330 (1994)
31 V.P. Kandidov, O.G. Kosareva, S.A. Shlenov: Quantum Electron. **24**, 905 (1994)
32 S.L. Chin, N. Aközbek, A. Proulx, S. Petit, C.M. Bowden: Opt. Commun. **188**, 181 (2001)